

Computational Simulation of Connectivity in the Brain Using Full Diffusion Tensor from MRI

Q. Yu* F. Liu* I. Turner* V. Vegh†

21 October 2010

Abstract

Diffusion tensor magnetic resonance imaging (DT-MRI) is a technique used to measure the diffusion properties of water molecules in tissues [1]. Anisotropic diffusion can be described by the equation

$$\frac{\partial C}{\partial t} = \nabla \cdot (D \nabla C)$$

where C is the concentration of water molecules and D is the diffusion tensor. The anisotropy of the diffusion tensor is of particular interest in brain images, as it is related to fibre tracts in white matter. Depending on the interrelation of the eigenvalues λ_i of D , diffusion can be divided into the three different cases of linear diffusion, planar diffusion and spherical diffusion.

In this paper we present additional information from the brain image (DT-MRI) of a patient with Parkinson's disease. This information includes maps of diffusion tensor components (DTC), fractional anisotropy (FA), relative anisotropy (RA), volume ratio (VR), tensor trace (TT) and FA-weighted colour-coded orientation. We also propose computational simulations of connectivity in the brain using numerical methods for the analysis of DT-MRI. This method involves solving a diffusion equation based on the measured diffusion tensor, where the initial condition is taken as a seed at a location used as a starting point in tractography. The seed diffuses through the brain,

*Discipline of Mathematical Sciences, Queensland University of Technology, Brisbane, AUSTRALIA. <mailto:f.liu@qut.edu.au>

†University of Queensland

and the amount at some position is interpreted as a probability to reach that point, given the input data. The model calculates connection probabilities between points of interest, which can be compared within or between subjects [2].

Contents

1	Introduction	2
2	Data Acquisition	4
3	Application	4
3.1	Diffusion Tensor Components	4
3.2	Anisotropies	5
3.3	Fitting white matter FA frequency	6
4	One-dimensional Models	6
4.1	Model 1: linear diffusion	7
4.2	Model 2: anomalous subdiffusion (time-fractional)	8
4.3	Model 3: space-fractional diffusion	10
5	Conclusions	11

1 Introduction

Diffusion tensor magnetic resonance imaging (DT-MRI) is a technique used to measure the diffusion properties of water molecules in tissues [1]. In white matter, which is one of the two components of the central nervous system and consists mostly of myelinated axons, the diffusion of free water molecules is anisotropic and such diffusion can be modelled by the equation

$$\frac{\partial C}{\partial t} = \nabla \cdot (D \nabla C), \quad (1)$$

where C is the concentration of water molecules and D is the usual symmetric second-rank diffusion tensor.

A property of second-rank tensors is that they can always be orthogonally diagonalized as $D = E \Lambda E^T = \sum_{i=1}^3 \lambda_i e_i e_i^T$ with $E = [e_1 \ e_2 \ e_3]$ and $\Lambda = \text{diag}(\lambda_1, \lambda_2, \lambda_3)$. The eigenvalues reflect the shape or configuration of an ellipsoid with surface representing the root mean square diffusive displacement of free water in anisotropic media. The sum (tensor trace(TT)

$= \lambda_1 + \lambda_2 + \lambda_3$), which is independent of the orientation of the ellipsoid (rotationally invariant), reflects the size of the ellipsoid. The mathematical relationship between the principal coordinates of the ellipsoid and the laboratory frame is described by the eigenvectors (e_1, e_2, e_3) .

In general, the eigenvalues are sorted with the convention that $\lambda_1 \geq \lambda_2 \geq \lambda_3$. Consequently, the first eigenvector e_1 describes the predominant diffusion direction and is therefore also called the Principal Diffusion Vector (PDV) or Principal Diffusivity (PD).

Depending on the interrelation of the eigenvalues λ_i of D , diffusion can be divided into three different cases, i.e. linear diffusion (the cigar-shaped ellipsoid)

$$\lambda_1 \gg \lambda_2 \approx \lambda_3 \quad \rightarrow \quad D \approx \lambda_1 e_1 e_1^T, \quad (2)$$

planar diffusion (the disc-shaped ellipsoid)

$$\lambda_1 \approx \lambda_2 \gg \lambda_3 \quad \rightarrow \quad D \approx \lambda_1 \sum_{i=1}^2 e_i e_i^T, \quad (3)$$

and spherical diffusion (the sphere-shaped ellipsoid)

$$\lambda_1 \approx \lambda_2 \approx \lambda_3 \quad \rightarrow \quad D \approx \lambda_1 \sum_{i=1}^3 e_i e_i^T. \quad (4)$$

The anisotropy of the diffusion tensor is of particular interest in brain images, as it is related to fibre tracts in white matter. Several measures of diffusion anisotropy, including fractional anisotropy (FA), relative anisotropy (RA), and volume ratio (VR), can be calculated from the eigenvalues as follows [5]

$$FA = \sqrt{\frac{1}{2} \frac{\sqrt{[(\lambda_1 - \lambda_2)^2 + (\lambda_2 - \lambda_3)^2 + (\lambda_3 - \lambda_1)^2]}}{\sqrt{\lambda_1^2 + \lambda_2^2 + \lambda_3^2}}}, \quad (5)$$

$$RA = \sqrt{\frac{1}{2} \frac{\sqrt{[(\lambda_1 - \lambda_2)^2 + (\lambda_2 - \lambda_3)^2 + (\lambda_3 - \lambda_1)^2]}}{\lambda_1 + \lambda_2 + \lambda_3}}, \quad (6)$$

$$VR = \frac{\lambda_1 \lambda_2 \lambda_3}{[(\lambda_1 + \lambda_2 + \lambda_3)/3]^3}. \quad (7)$$

Orientation-map images, represent the direction of the maximum eigenvector, coloured according to the eigenvector direction and scaled by multiplying the eigenvector direction cosine with the fractional anisotropy.

In this paper we first show some information including the maps of diffusion tensor components, FA, RA, VR, TT, and the eigenvalues and FA-weighted color-coded orientation that can be derived from the diffusion tensor. Then, some models relating to linear diffusion are presented.

2 Data Acquisition

The data we use here is from a 64-year-old patient having Parkinson's disease captured before and after surgery. The brain diffusion tensor MR images are generated on a GE Medical System (SIGNA 3T) scanner. All image matrix sizes are 256×256 .

Before surgery the echo time is fixed at 93.7 msec, whereas the repetition time is fixed at 7000 msec. Twenty four interleaved, 5-mm-thick slices are acquired in the axial plane using the multislice mode. Diffusion sensitization is performed along 35 different diffusion gradient orientations using a diffusion weighting of $b = 1000 \text{ sec/mm}^2$. A reference image without diffusion weighting ($b = 0 \text{ sec/mm}^2$) is also recorded.

After surgery the echo time is fixed at 93.5 msec, and the repetition time is fixed at 7000 msec. In addition, 26 interleaved, 5-mm-thick slices are acquired in the axial plane using the multislice mode. Furthermore, diffusion sensitization is performed along 40 different diffusion gradient orientations using a diffusion weighting of $b = 1000 \text{ sec/mm}^2$. Similarly, a reference image without diffusion weighting ($b = 0 \text{ sec/mm}^2$) is also recorded.

3 Application

3.1 Diffusion Tensor Components

The images shown in Figures 1-2 depict the diffusion tensor components (D_{xx} , D_{xy} , D_{xz} , D_{yy} , D_{yz} , D_{zz}) determined prior to and post surgery respectively. One notes the changes in the tensor components after surgery, particularly in the diagonal entries where the distinct central structure is no longer evident.

Figure 3 depicts the change in the eigenvalues after surgery. The largest, middle and smallest eigenvalues are shown before surgery in (a, b, c) and after surgery in (d, e, f) respectively. Clearly, the surgical procedure has had a significant impact on the eigenvalue distributions, again most notably around the central structure.

In Figure 4 (a) and (b) we have displayed images of the brain before and after surgery respectively. On these images we have marked locations A, B, C based on the diffusion cases identified according to the magnitude of the eigenvalues (see equations 2, 3, 4). It is interesting to note that point A, before surgery, was classified as linear diffusion, whereas after surgery it moves to spherical diffusion. Note also, point B changes from spherical to planar diffusion after surgery, while point C is unchanged. These findings may be helpful to the surgeon treating the patient.

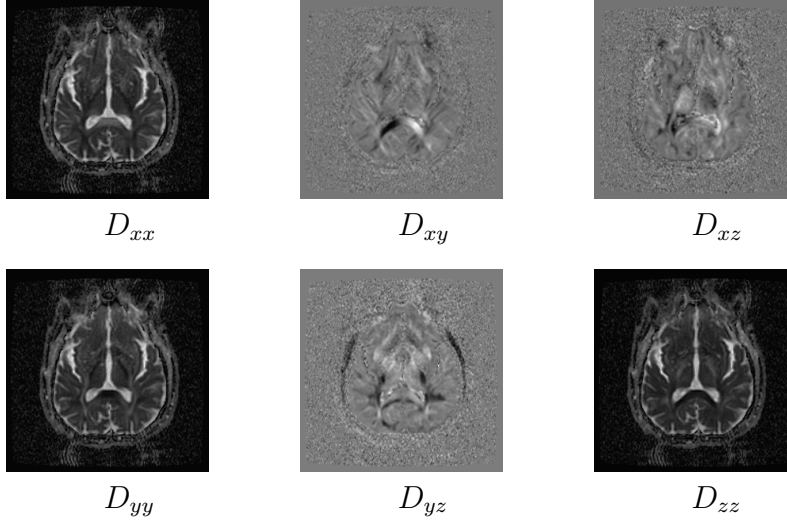


Figure 1: Diffusion tensor components before surgery

Table 1: Eigenvalues at the same points in white matter(WM) before and after the surgery

WM	Eigenvalues(presurgical)	Eigenvalues(postsurgical)
A(142,164)	(1.661E-3, 3.08E-4, 2.51E-4)	(1.337E-3, 1.03E-3, 9.22E-4)
B(91,143)	(6.06E-4, 5.59E-4, 4.22E-4)	(1.1E-3, 1.05E-3, 5.5E-4)
C(142,90)	(1.169E-3, 8.41E-4, 5.2E-4)	(2.392E-3, 1.276E-3, 6.33E-4)

3.2 Anisotropies

In Figure 5, we display some of the classical anisotropies RA, FA and VR, with the tensor trace (TT) image. The trends in the images after surgery are consistent with those observed in Figures 1-3.

Figure 6 shows color-coded orientation-map images representing the direction of the maximum eigenvector with their intensities weighted by FA. The color-coded orientation maps with the largest, middle and smallest eigenvalues are shown before surgery in (a, b, c) and after surgery in (d, e, f) respectively. In this figure, red represents the eigenvector direction perpendicular to the image plane, green represents left-to-right and blue represents up-and-down. Obviously, the surgical procedure has altered the maximum eigenvector direction distributions.

As can be seen from the image in Figure 8(a), the mean FA values of patient were lower before surgery, however the mean FA values of a normal adult are 0.68 ± 0.18 . Note that the data of a normal adult are reproduced

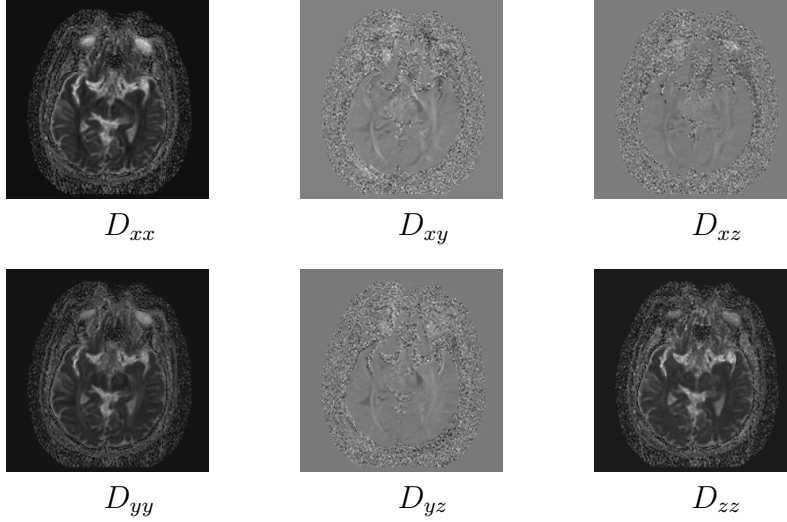


Figure 2: Diffusion tensor components after surgery

from [5]. Figure 8(a) clearly shows that the surgery produces a mean FA value closer to that observed for a normal adult.

3.3 Fitting white matter FA frequency

From [6], we found that a mixture of two distributions, a normal distribution and the inverse Gaussian distribution, can be used to fit the distribution of the whole brain white matter fractional anisotropy (FA) frequency.

Figure 7 clearly shows the postsurgical whole brain white matter fractional anisotropy distribution (PostWM-FAD) to be positively skewed and leptokurtic, whereas the presurgical whole brain white matter fractional anisotropy distribution (PreWM-FAD) is positively skewed and less leptokurtic than the PostWM-FAD. Furthermore, there is an interaction between the measured histogram parameters, see for example the PostWM-FAD, which is highly leptokurtic having a greater peak height frequency than the PreWM-FAD, while the PostWM-FAD also has a greater positive skew being more asymmetrical than the PreWM-FAD.

4 One-dimensional Models

When the diffusion is linear, planar and spherical, the corresponding diffusion equation (1) becomes one-dimensional, two-dimensional and three-

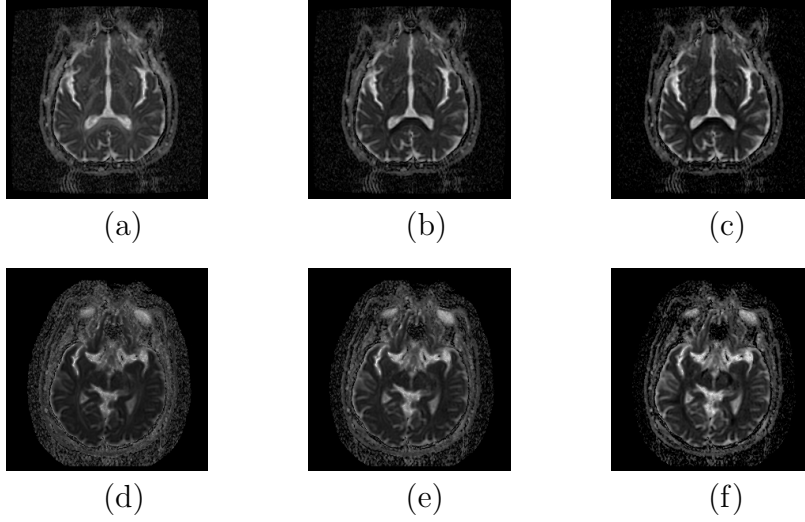


Figure 3: Eigenvalues. Top row is presurgical and bottom row is postsurgical.

dimensional respectively.

The aim of this section is to illustrate how the diffusion tensor information could be used to model the diffusion behaviour in the white matter of the brain. The models we investigate will be standard diffusion, anomalous subdiffusion and fractional-in-space diffusion. Because the white matter is highly heterogenous we believe that non-Fickian diffusion will be evident. The computed solutions are obtained by injecting a surgical treatment at a particular location within the brain.

In this paper, we only show some numerical results of the one-dimensional model with initial condition given by the dirac delta function $\delta(x)$ with Neumann boundary conditions using finite difference methods (FDM) [7, 8]. We have obtained similar results using finite element methods (FEM). The two-dimensional and three-dimensional models can be similarly simulated and their solutions will be exhibited in future work.

4.1 Model 1: linear diffusion

When the diffusion is linear, applying (2) the equation (1) becomes the well-known standard diffusion equation (SDE):

$$\frac{\partial C}{\partial t} = D \frac{\partial^2 C}{\partial x^2}, -L \leq x \leq L, 0 \leq t \leq T. \quad (8)$$

The solution profiles of SDE with $L = 5$ and $D = 1$ are shown in Figure 8(b).

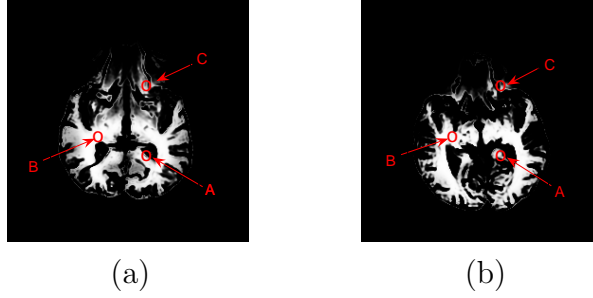


Figure 4: Three eigenvalues in white matter, (a) presurgical and (b) postsurgical.

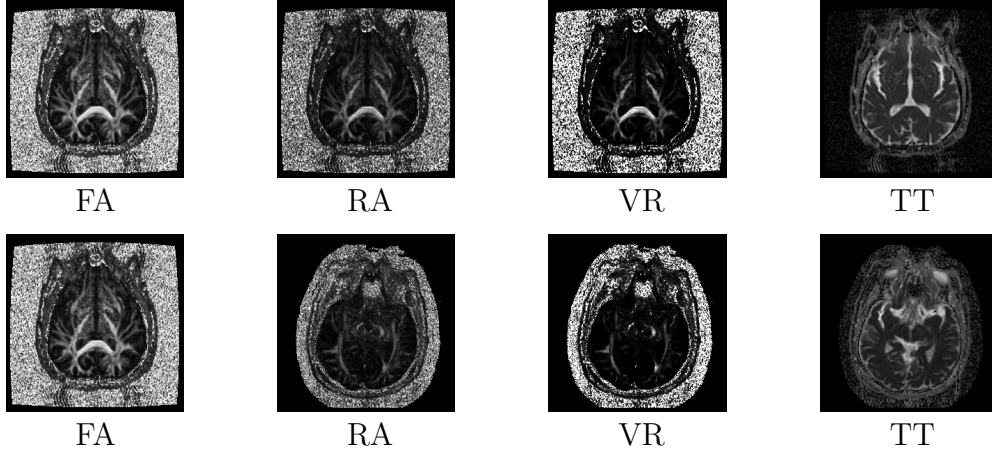


Figure 5: The anisotropy indices and the tensor trace. Top row is presurgical and bottom row is postsurgical.

4.2 Model 2: anomalous subdiffusion (time-fractional)

Fractional kinetic equations have proved particularly useful in the context of anomalous subdiffusion [9]. The mean square displacement of the particles from the original starting site is no longer linear in time and follows a generalized Ficks second law. Subdiffusive motion is characterized by an asymptotic long-time behavior of the mean square displacement of the form

$$\langle x^2(t) \rangle \sim \frac{2K_\gamma}{\Gamma(1+\gamma)} t^\gamma, \quad t \rightarrow \infty, \quad (9)$$

where γ (with $0 < \gamma < 1$) is the anomalous diffusion exponent and K_γ is the generalized diffusion coefficient. Ordinary (or Brownian) diffusion corre-

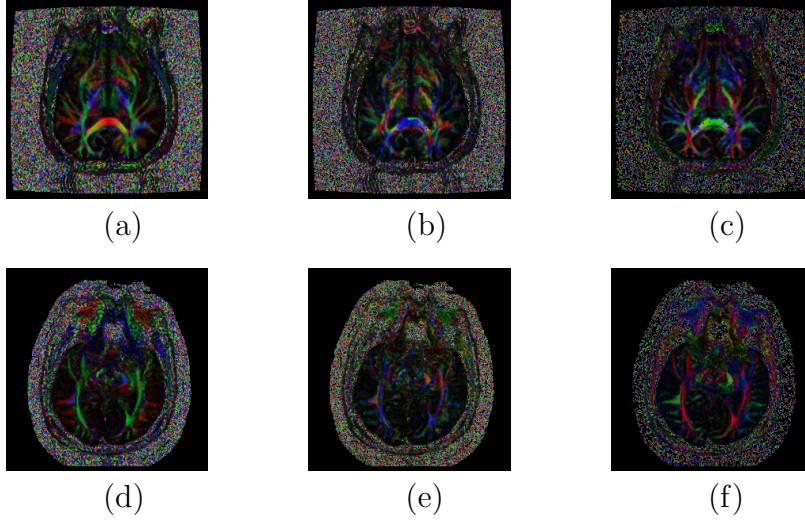


Figure 6: FA-weighted color-coded orientation maps. Top row is presurgical and bottom row is postsurgical.

sponds to $\gamma = 1$ with $K_1 = D$ (the ordinary diffusion coefficient).

For anomalous subdiffusive random walkers, the continuum description via the ordinary diffusion equation is replaced by the fractional diffusion equation. It has been suggested that the probability density function $C(x, t)$ that describes anomalous subdiffusion particles follows the anomalous subdiffusion equation (AS-DE) [9]:

$$\frac{\partial C}{\partial t} = D_t^{1-\gamma} [K_\gamma \frac{\partial^2 C}{\partial x^2}], -L \leq x \leq L, 0 \leq t \leq T, 0 < \gamma \leq 1, \quad (10)$$

where $C(x, t)$ is the probability density and $D_t^{1-\gamma}$ is the Riemann-Liouville time fractional derivative which is defined as [7]

$$D_t^{1-\gamma} f(x, t) = \begin{cases} \frac{1}{\Gamma(\gamma)} \frac{\partial}{\partial t} \int_0^t \frac{f(x, \xi) d\xi}{(t-\xi)^{1-\gamma}}, & 0 < \gamma < 1, \\ \frac{\partial f(x, t)}{\partial t}, & \gamma = 1. \end{cases} \quad (11)$$

The evolution results of AS-DE with $L = 5, K_\gamma = 1$ are shown in Figure 9(a). From Figure 9(a), it can be seen that the system exhibits subdiffusion behaviors, and the solution continuously depends on the time fractional derivative.

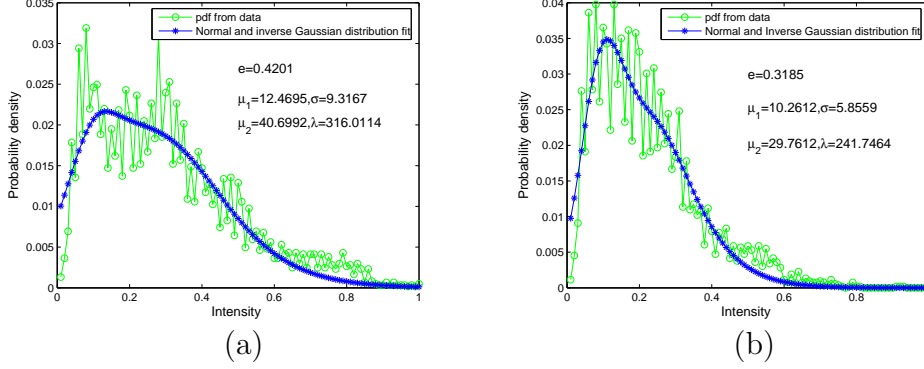


Figure 7: Whole brain white matter fractional anisotropy (FA) frequency after fitting with different probability density function (PDF) range, (left) presurgical, (right) postsurgical.

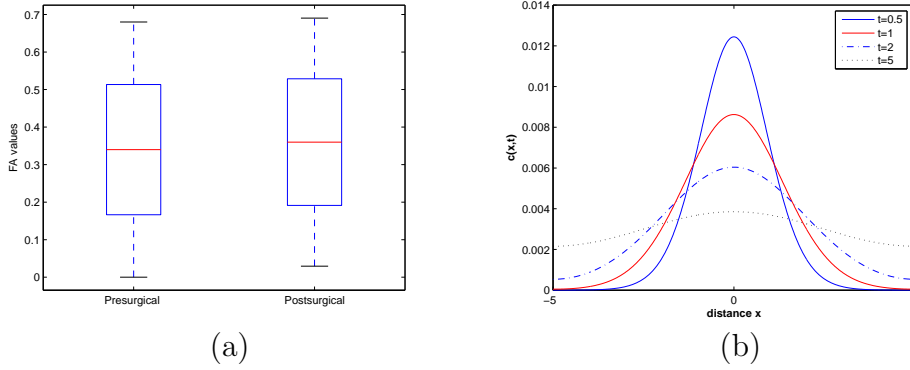


Figure 8: (a) Mean FA values; (b) solution profiles of SDE as a function of x for different t .

4.3 Model 3: space-fractional diffusion

Because the white matter is highly heterogeneous, the traditional standard diffusion equation may not be adequate. The heterogeneity of the white matter may alter the laws of Markov diffusion in a fundamental way. If the complex structure, such as the spatial connectivity, can facilitate movement of particles within a certain scale, fast motions may no longer obey the classical Fick's law and may indeed have a probability density function that follows a power-law. Superdiffusion is one possible form of fast motions.

Fractional derivatives play a key role in modelling particle transport in anomalous diffusion. By replacing the second space derivative by a fractional derivative of order α , $1 < \alpha \leq 2$, the classical diffusion equation SDE becomes

a one-dimensional space fractional diffusion equation (SF-DE):

$$\frac{\partial C}{\partial t} = D \frac{\partial^\alpha C}{\partial x^\alpha}, -L \leq x \leq L, 0 \leq t \leq T, 1 < \alpha \leq 2, \quad (12)$$

where $\frac{\partial^\alpha}{\partial x^\alpha}$ is the Riemann-Liouville space fractional derivative, which is defined as [8]

$$\frac{\partial^\alpha f(x, t)}{\partial x^\alpha} = \begin{cases} \frac{1}{\Gamma(2-\alpha)} \frac{\partial^2}{\partial x^2} \int_0^x \frac{f(\xi, t) d\xi}{(x-\xi)^{\alpha-1}}, & 1 < \alpha < 2, \\ \frac{\partial^2 f(x, t)}{\partial x^2}, & \alpha = 2. \end{cases} \quad (13)$$

Figure 9(b) shows the solution profiles of SF-DE with $L = 5$, $D = 1$. From Figure 9(b), it can be seen that the system exhibits diffusion behaviors such that the solution continuously depends on the space fractional derivative.

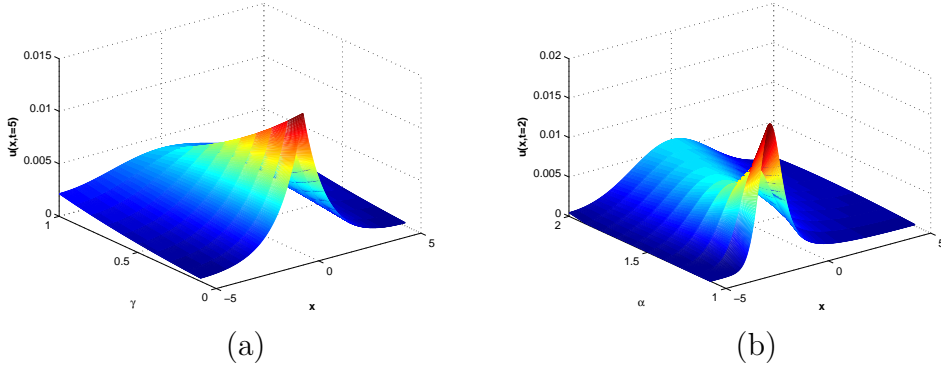


Figure 9: (a) Numerical results of AS-DE at $t = 5$; (b) numerical results of SF-DE at $t = 2$.

5 Conclusions

We have derived numerical methods to analyse brain images and develop one-dimensional fractional models to study anomalous diffusion behaviour in the white matter of the brain. In addition, brain image data has been compared for a patient with Parkinson's disease before and after surgery. We believe that the simulated information can be used to the surgeon treating the patient.

Acknowledgements: The authors gratefully acknowledge the help of Professor Kerrie Mengersen, Professor Kevin Burrage and phd student Nicole White, and thank the assistance of Professor Peter Silburn, Neurology Department, St Andrew's Hospital, Australia for the data acquisition.

References

- [1] P. G. Batchelor, D. L. G. Hill, F. Calamante and D. Atkinson, Study of connectivity in the brain using the full diffusion tensor from MRI. *Proceedings of Information Processing in Medical Imaging IPMI*, 2082: 121-133, 2001.
- [2] L. Zhukov, K. Museth, D. Breen, R. Whitaker, A. Barr, Level set modeling and segmentation of DT-MRI brain data. *Journal of Electronic Imaging*, 12(1): 125-133, 2003.
- [3] E. R. Melhem, S. Mori, G. Mukundan, M. A. Kraut, M. G. Pomper and P. C. M. van Zijl, Diffusion Tensor MR Imaging of the Brain and White Matter Tractography , *Review*, 178: 3-16, 2002.
- [4] A. Leemans, Modeling and processing of diffusion tensor magnetic resonance images for improved analysis of brain connectivity. *PhD thesis*, 2006.
- [5] S. Mori, *Introduction to Diffusion Tensor Imaging*. Elsevier B.V., 2007.
- [6] Z. Zhao, Z. G. Yu, V. V. Anh, Topological properties and fractal dimension of the Sierpinski and generalized Sierpinski networks. *Commun. Frac. Calc.*, 1: 15-26, 2010.
- [7] P. Zhuang, F. Liu, V. Anh and I. Turner, New solution and analytical techniques of the implicit numerical methods for the anomalous sub-diffusion equation. *SIAM J. on Numerical Analysis*, 46(2): 1079-1095, 2008.
- [8] F. Liu, V. Anh, I. Turner Numerical solution of the space fractional Fokker-Planck equation. *Journal of Computational and Applied Mathematics*, 166: 209-219, 2004.
- [9] R. Metzler and J. Klafter, The random walks guide to anomalous diffusion: A fractional dynamics approach, *Phys. Rep.*, 339: 1C77, 2000.